



Research papers

Identification of non-Darcian flow effect in double-porosity fractured aquifer based on multi-well pumping test



Yilin Wang ^a, Hongbin Zhan ^{b,*}, Kun Huang ^a, Linqing He ^c, Junwei Wan ^{a,*}

^a School of Environmental Studies, China University of Geosciences, Wuhan, Hubei 430074, PR China

^b Department of Geology and Geophysics, Texas A & M University, College Station, TX 77843-3115, USA

^c Changjiang Institute of Survey Technical Research, MWR, Wuhan, Hubei 430074, PR China

ARTICLE INFO

Keywords:

Multi-well pumping test
Double-porosity medium
Non-Darcian flow
Izbash equation
Parameter inversion
Particle swarm optimization

ABSTRACT

Well testing in double-porosity fractured aquifers or oil and gas reservoirs is one of the long-lasting research problems in subsurface hydrology and petroleum engineering, where the double-porosity implies that the media of concern can be approximated as a two interrelated continua (fracture network and rock matrix) with two distinctively different porosities. However, most of those studies in double-porosity fractured aquifers only concern Darcian flow in the fractured continuum. In this study, we will expand such studies from Darcian flow regime to non-Darcian flow regime, which is most likely to be the case for the field well testing site reported in this investigation. New solutions based on power law and a linearization approximation are obtained for hydraulic heads in Laplace domain and subsequently inverted to give spatiotemporal distributions in real-time domain. The non-Darcian flow model in single porosity media is obtained by setting the leakage coefficient (C) to 0 or the storage coefficient of the matrix (S_m) to 0, where C is the rate of fluid transfer between the fracture and rock matrix. Parameter analysis is conducted using dimensionless formats. A larger dimensionless quasi conductivity coefficient K_{qD} , a larger drawdown in the early stage, and a smaller drawdown in the late stage. The dimensionless parameters C_D and ϕ influence the drawdown in transitional state, and the values get larger, the drawdown in transitional state drop smaller. A pumping test conducted in Huangtun, Anhui province of China has been applied to test the non-Darcian flow effect in a double-porosity aquifer, in which a particle swarm optimization (PSO) algorithm will be applied here to seek the optimal hydraulic parameters. As the result shows, the observed drawdown data fit well with the new model in the pumping stage. The predicted recovery drawdown curve with the calculated parameters of the new model also performs well with the field drawdown data, which supports the applicability of the new model to interpret the field data.

1. Introduction

Subsurface fluid flow (either in single-phase or multi-phase) in fractured media is an important and long-lasting subject for geoscientists and petroleum engineers, such as water resource management (Papadopoulou et al., 2009), geothermal energy development (Cook, 1992, Kishida et al., 2013, Min et al., 2009), petroleum exploration and production (Camac et al., 2006, Karpyn et al., 2009) and underground tunnel excavation (Molinero et al., 2002, Ren et al., 2015). In recent decades, researchers have made significant efforts to understand this issue and realized that the fractured media of concern may have to be approximated using multiple interrelated continua such as double-porosity, triple-porosity, double-permeability, triple-permeability, etc.

(Jenkins and Prentice, 1982, Kohl et al., 1997, Quinn et al., 2011, Radilla et al., 2013). Laboratory experiments (Li et al., 2017, Li et al., 2019, Qian et al., 2005, Rong et al., 2017), field tests (Quinn et al., 2013) and numerical simulations (Smaoui et al., 2012, Wang et al., 2013, Zhang et al., 2019) have been utilized extensively to investigate such an issue. The double-porosity model may be regarded as a subset of the double-permeability model as it approximates the rock matrix permeability as almost negligible, meaning that flow among different rock matrix is not permitted unless it is through the fracture. Similarly, the triple-porosity model may be regarded as the subset of triple-permeability model as well as it regarded the permeability values in the low-permeability media as zeros as well. Regardless of the complexity associated with flow in a fractured media, Darcy's law is the

* Corresponding authors.

E-mail addresses: zhan@geos.tamu.edu (H. Zhan), wanjw@cug.edu.cn (J. Wan).

primary law used for describing flow in those continua associated with the fracture media. However, it is confirmed that flow in fracture or coarse granular porous media sometime deviates noticeably from Darcy's law at high velocities (or more specifically, high Reynolds numbers) of flow (Banerjee et al., 2017, Cherubini et al., 2012, Li et al., 2019, Qian et al., 2015, Qian et al., 2007, Zoorabadi et al., 2015). This is primarily because the inertial effect that is neglected in Darcy's law becomes increasingly prominent and non-negligible when the flow velocities (or Reynolds numbers) in those media become sufficiently high, which is very likely to occur in the fractured network under certain circumstances. On the other end, in some much less permeable rock matrix (as in dual-permeability and triple-permeability frameworks instead of double-porosity and triple-porosity frameworks in which direct flow communication between rock matrixes is prohibited unless it is through the fracture network), Darcy's law may also break down when a threshold hydraulic gradient is required to mobilize fluid flow there. This is mainly caused by various driving forces in addition to the viscous force (which is the primary driving force for Darcian flow) such as electric forces caused by surface charges, forces associated with chemical potentials (Bolt and Groenevelt, 1969, Neuzil, 1986), etc.

Flow starts to deviate from Darcian flow regime when Reynolds number starts to increase, a non-Darcian flow law is needed when the Reynolds number exceeds the critical Reynolds number, which is a representative Reynolds number separating the Darcian flow regime from the non-Darcian flow regime (Qian et al., 2005, Xia et al., 2017). The critical Reynolds number should be understood as a representative number (or the average Reynolds number) within a transitional range, in which the transition from Darcian flow to non-Darcian flow happened smoothly. In respect of the candidate equations for describing non-Darcian flow, Forchheimer law (or second-order polynomial function) (Forchheimer, 1901) and Izbash law (or power law) (Izbash, 1931) are two of the most popular ones (Sen, 1987, Tzelepis et al., 2015, Wu, 2002, Zhu and Wen, 2020). In the Forchheimer law, the hydraulic gradient is a second-order polynomial function of flow rate (or specific discharge), and the linear term and the quadratic term describe the energy losses due to viscous and inertial dissipation mechanisms, respectively (Cherubini et al., 2013, Javadi et al., 2014, Sen, 1987, Wu, 2002). In the Izbash law, the hydraulic gradient is an empirical power-law function of the flow rate (Chen et al., 2015, Soni et al., 1978). For instance, Sen (1987) characterized the non-Darcian flow in a planar fracture by the Forchheimer law. Cherubini et al. (2013) carried out laboratory hydraulic tests in an artificially created fractured rock, and confirmed the validity of Forchheimer law. Soni et al. (1978) applied the Izbash law to the constant-head permeameter tests in coarse-grained porous media with satisfactory. Liu et al. (2016) presented a fractal Izbash law-based analytical model for data interpretation of constant-rate tests in a fractured crystalline aquifer and concluded that the power index could be understood as a phenomenological approximation of flow with some sorts of average in the region not so far away from the pumping well. For some cases, both Forchheimer law and Izbash law are equally acceptable to describe flow in a fractured media (Bordier and Zimmer, 2000, Qian et al., 2011, Xia et al., 2017). The Izbash law has been criticized for not describing the far-field (the field far from the pumping or injection wells) very well because flow in those regions is assumed to follow the Darcy's law. Such a criticism has been reconciled in a number of studies before (Xiao et al., 2019). Furthermore, from a practical point of view, the data that are most important for pumping test interpretation are not collected from the far-field (in which the drawdown response is too weak). Much detailed discussion on the rationale of using the Izbash equation for this study will be documented in section 2.3 based on the analysis of the pumping test data.

When a fractured medium is characterized as double-porosity, the primary porosity rock matrix continuum is usually characterized as of low (almost negligible) permeability and high storage capacity, and the secondary porosity fracture network continuum is characterized as of high permeability and low storage capacity (Barenblatt et al. 1960,

Moench 1984, Warren and Root 1963). Fluid can transfer between these two continua but no fluid exchange can happen between neighboring rock matrix blocks (without involving fractures) (De Smedt 2011). In the previous studies, it was considered that the flows in the fracture continuum followed Darcy's law (De Smedt 2011, Hamm and Bidaux 1996, Kaczmaryk and Delay 2007, Kazemi and Seth 1969). However, it is noteworthy that the non-Darcian flow effect appears in the fracture continuum quite easily (Altinors and Onder, 2008). For example, Kohl et al. (1997) used numerical simulation to investigate a fracture-matrix flow system with non-Darcian fracture flow, which can well explain the hydraulic production and injection experiments conducted at the Soulitz hot dry rock test site. Wu (2002) employed the Forchheimer law to describe the non-Darcian flow through fractures in a double-porosity framework, and derived a steady-state analytical solution for the spatial distribution of the hydraulic head. Altinors and Onder (2008) expanded the Forchheimer law in a fractured aquifer bounded by a stream. Zhang (2020) developed a anisotropic double-porosity elasto-plastic framework which considered both Darcian flow and non-Darcian flow in fissured rock and Zhang et al. (2021) extended it to a double-porosity media with ultra-low matrix permeability. Overall, there are more modeling studies concerning non-Darcian flow in a fractured media, but very few field tests to confirm those modeling exercises to access the importance of non-Darcian flow effect in fractured media.

Huangtun, located in Anhui province, China, is an area that has undergone multiple periods of tectonic activity and magma intrusion. The Jurassic Andesite stratum is supposed to be low-permeability in nature before it was reconstructed by tectonic activity. Whereas, the initial stratum is intersected by faults to generate fractures, resulting in the stratum functioning as a double-porosity media as the fractures or fissures enhance the permeability of stratum. Rapid response to hydraulic stress (recharge events, pumping tests) is common in a fracture network which is dominated by preferential flow through the low-storage, high-permeability fracture, in which non-Darcian flow is prone to occur because of the highly permeable nature of fractures (Worthington et al., 2019). Hence, it is worthwhile to investigate how the non-Darcian flow regime in fracture affects the hydraulic responses in pumping tests conducted in a double-porosity media. However, despite of its obvious importance, field studies associated with non-Darcian flow in a double-porosity media is very rare up to present. The Huangtun field site investigated in this study provides a much-needed opportunity for such a purpose because of its double-porosity nature.

To sum up, the objective of this work is to present a comprehensive field well test conducted in a fractured aquifer to demonstrate the unique features of well testing in an actual fractured media that may be approximated as a double-porosity media. After this, we will search for a proper mathematical model to interpret the data collected from the tests. Lastly, we will introduce a particle swarm optimization (PSO) algorithm to conduct a parameter estimation exercise based on the inverse modeling of the established forward mathematical model of flow.

2. Material and method

2.1. Study area

The field test site is situated 30 km northeast of Lujiang County, Anhui Province of China, in the middle of Yangtze River (Fig. 1a). The study area is located in the upstream portion of the Huangtun River alluvial plain. The area has a typical subtropical humid monsoon climate and a mean annual temperature of 15.6°C. According to the observation data of Lujiang meteorological station, the average annual precipitation is 1258.94 mm, most of the annual precipitation falls during the rainy season from May to August, while the average annual surface-water evaporation is 1353.14 mm.

The field site has a three-layer structure, with Quaternary on the top, Jurassic in the middle and Triassic in the bottom. The clay of poor

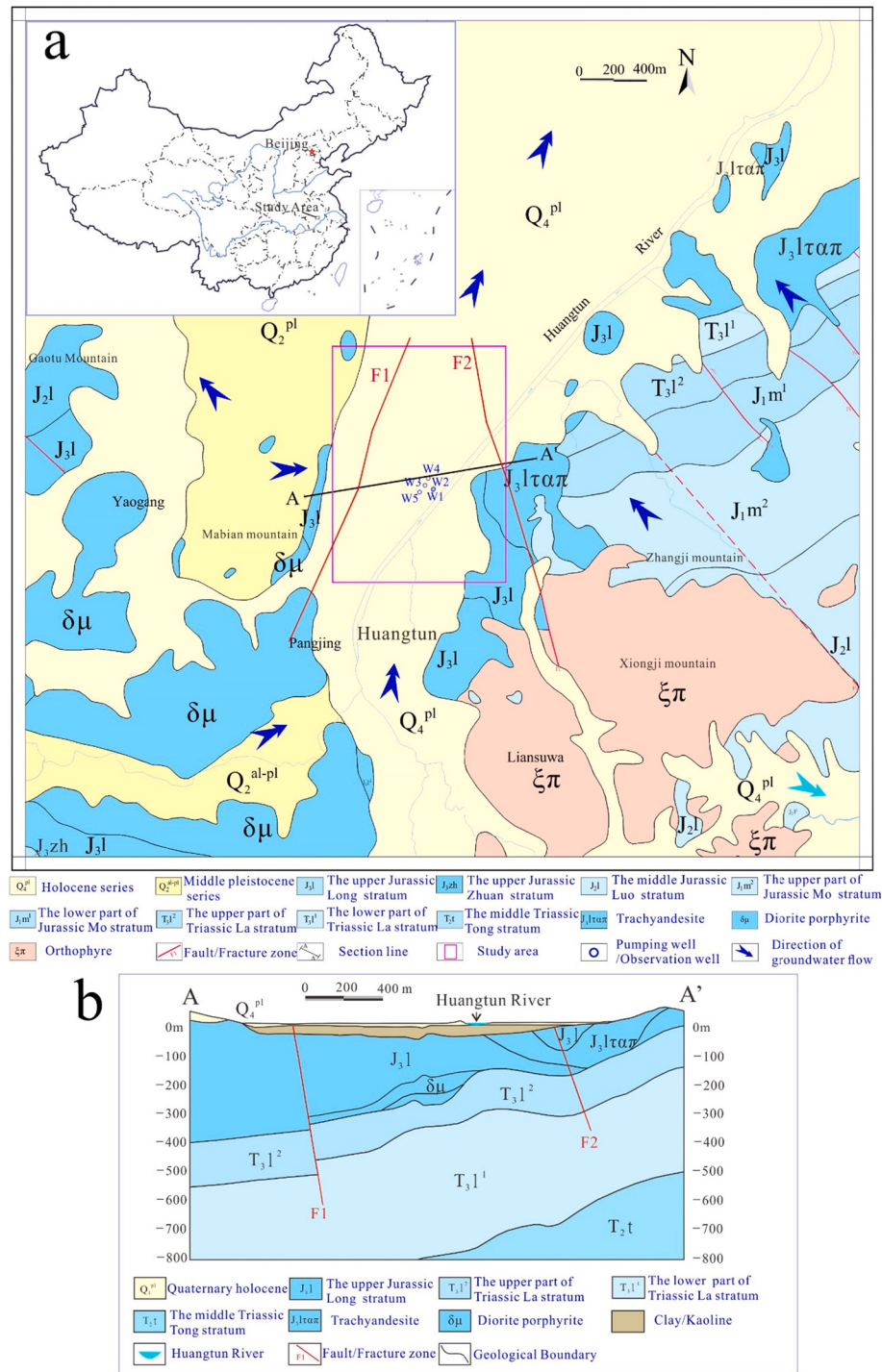


Fig. 1. Location of the field site and Wells distribution (a), the hydrogeological profile for section line A-A' (b).

permeability forms the Quaternary formation, which cut off the hydraulic connection of surface water (Huangtun River) and subsurface groundwater (the Jurassic aquifer), is considered as an aquiclude. The Jurassic stratum mainly consisting of Andesite with a thickness of about 250 m (Fig. 1b) is the main aquifer in the study area. The lithology of the Triassic stratum is mainly quartz sandstone, and this stratum is considered as aquiclude because of its poorly developed fracture. According to field geological and geophysical survey, there is a fault on the east and west sides of the study area, the fault F1 on the west side is a reverse fault with a length of more than 1200 m and a dip angle of about 70-90°; the fault F2 on the east side is a translational fault with a length of more than 1200 m and a dip angle of about 63-74°. Due to the

influence of diagenesis and tectonic activities, the Jurassic volcanic rocks develop both small pores and fractures, as confirmed by core samples excavated from this stratum (Fig. 2).

2.2. Multi-well pumping test

A multi-well pumping test has been designed to study the hydraulic characteristics of the Jurassic aquifer of concern. A pumping well (W1) runs through the Jurassic aquifer in the middle of the study area and four observation wells (W2-W5) are scattered around it (Fig. 1b). The nearest observation well is W2 at 5.57 m from the pumping well, and the farthest is W5 at 81.91 m from the pumping well. W3 and W4 are away

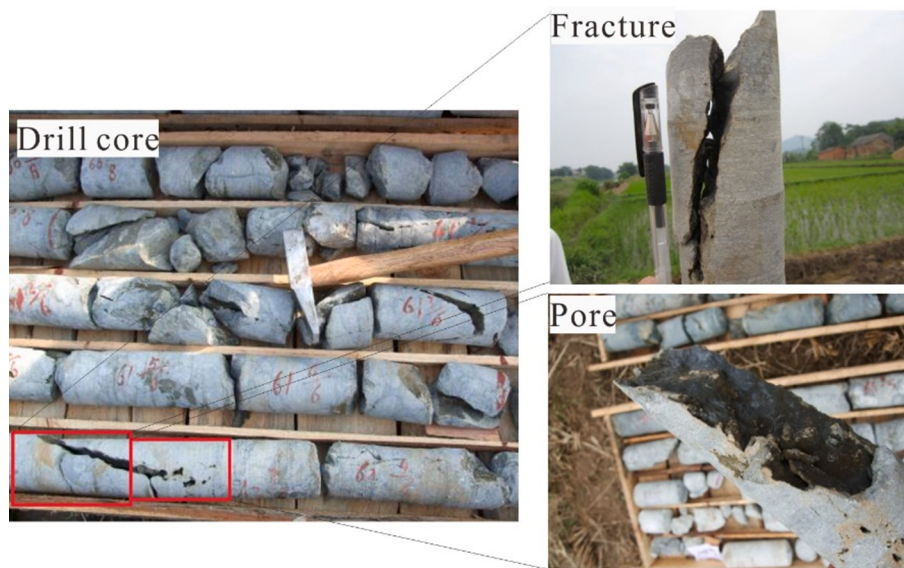


Fig. 2. The picture of drill core and examples of enlargement pore and fracture.

from pumping well for distance 54.84 m and 73.48 m, respectively. A deep mining dewatering well (W1) continues pumping about 2 h to generate considerable drawdown near the pumping well in the Jurassic aquifer (Fig. 3). The pumping rate measured by a triangular weir is similar to a constant-rate pump, and the pumping rate is determined to be $417 \text{ m}^3/\text{hr}$. The groundwater levels in the observation wells are monitored by automatic water level monitor (*Levelogger 3.0, $\pm 0.05\%$, Solinst, Canada*), with an inspection frequency of 20 s.

The drawdown-logarithmic time curves at observation wells are shown in Fig. 4. Among all the observation wells, it can be divided into two classes: one is the observation well W2 which is the closest to the pumping well W1 (with a radial distance of $r = 5.57 \text{ m}$), with the largest drawdown and showing a 'S-shape' curve; the rest is the other observation wells except W2, with relatively small drawdowns and showing monotonously increasing curves. Analyzing the drawdown of W2 over the entire pumping duration, one can see that at the beginning of the pumping, the water level in W2 drops rapidly; at about 6 min of pumping, the growth of drawdown slows down and the drawdown curve exhibits an inflection point; the drawdown increases rapidly again after the inflection point. The drawdown curve of W2 over the whole pumping time results in a 'S' shape, which is incongruent to the drawdown curve typically seen in homogeneous aquifers. At the end of pumping, the maximum drawdown is 2.89 m in W2. As the pumping

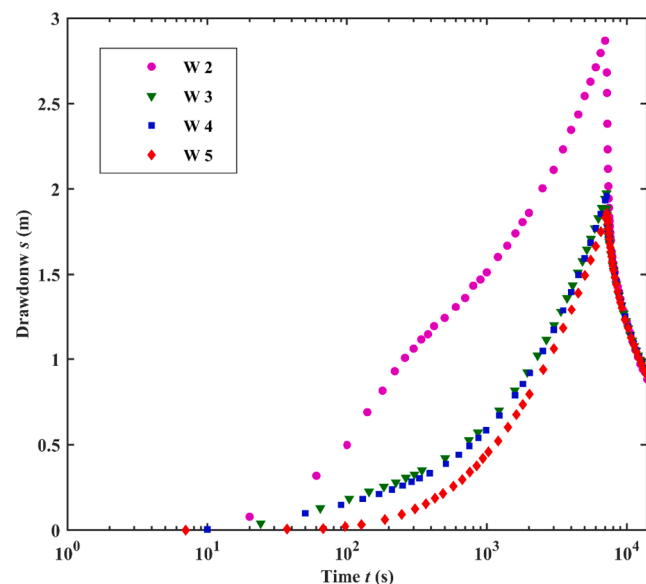


Fig. 4. Drawdown variations during the pumping and recovery time at observation wells.

time is limited to 2 h, no obvious water level drops have been observed near faults F1 and F2, implying that the groundwater depression cone has not yet reached the faults. In addition, there are little changes of water level in Quaternary borehole during the pumping time, indicating that the Jurassic aquifer can be considered as a confined aquifer owing to the weak connection with the upper water-bearing layer. The recovery time continues for 2 h to observe the water level change in the Jurassic aquifer. As Fig. 4 shows, during the limited recovery period, the water level in the four observation wells recovered from the maximum drawdown to the approximate drawdown about 0.8 m.

2.3. Mathematical formulation

The background hydraulic gradient at the field site is quite gentle before pumping, and the initial groundwater levels can be approximately treated as horizontal. The Jurassic aquifer contains well developed fractures and relatively intact rock matrixes, which may be



Fig. 3. Picture of the water outlet in the field pumping test.

conceptualized as a double-porosity media. The 'S-shaped' drawdown type curve observed in W2 is also supportive of the double-porosity media characteristics (Barenblatt et al., 1960, Moench, 1984, Warren and Root, 1963). During the pumping test, the groundwater flow rate changes rapidly and a considerable cone of depression develops because of the massive rate of withdrawal. Because of such a large rate of pumping, it is understandable that significant inertial energy losses may be generated in addition to the viscous energy losses, creating the non-Darcian flow near the pumping well in the fractured network. We have conducted numerous numerical exercises attempting to understand the drawdown type curves based on the single-porosity Darcian flow model (or the Theis model) or the double-porosity Darcian flow model and is generally unsuccessful. This forces us to look for either the single-porosity non-Darcian flow model, such as those of Wen et al. (2006) and Mathias et al. (2008) or the double-porosity non-Darcian flow model. The exercises of the single-porosity non-Darcian flow model are also unsatisfactory, which is understandable as the existence of fracture and rock matrix as two vastly different porosities is obvious. Therefore, we move on to search for a proper double-porosity non-Darcian flow model to understand the drawdown data. Among the two popular non-Darcian flow models (Forchheimer equation and Izbash equation), we find that the Izbash equation appears to work better for the case of concern here. The use of the Izbash equation is further discussed as follows.

Firstly, the key feature of non-Darcian flow (from a macroscopic perspective) is its deviation from the linear trend of the hydraulic gradient versus the specific discharge, and such a deviation has been described using many different functions by numerous scholars for many decades (Blick, 1966, Ergun, 1952, Forchheimer, 1901, Izbash, 1931, Macdonald et al., 1979). Among the vast number of functions proposed so far, two types of functions are most frequently used. One is the polynomial type functions, particularly the second-order polynomial function called the Forchheimer equation (Li et al., 2020a, Mathias and Moutsopoulos, 2016, Mathias and Todman, 2010, Quinn et al., 2020, Shi et al., 2020, Wang et al., 2014, Wen et al., 2011, Wen et al., 2014). The second is the power-law function called the Izbash equation (Bordier and Zimmer, 2000, Kang et al., 2011, Qian et al., 2018, Rong et al., 2016, Wen et al., 2013, Wen and Wang, 2013). Some scholars have stated that the Forchheimer equation is probably a better choice because it satisfies the two extremes of the non-Darcian flow, i.e., when the specific discharge is sufficiently small, it degenerates to Darcian flow, and when the specific discharge is sufficiently large, it degenerates to the fully developed turbulent flow (Balhoff et al., 2009, Banerjee and Pasupuleti, 2019, Sivanesapillai et al., 2014, Skjetne and Auriault, 1999, Zhou et al., 2015). However, satisfying the two extreme conditions (sufficiently small and sufficiently large specific discharges) does not necessarily mean that the function is the optimal choice for the intermediate range of the specific discharge between the two extremes. Furthermore, the effort of trying to connect the coefficients of Forchheimer equation with the fundamental aquifer parameters such as porosity, pore size distributions, pore geometry, heterogeneities, etc., is still far from successful. Indeed, active research on this subject is still going on (Li et al., 2020a, Li et al., 2019, Li et al., 2020b, Mwetulundila and Atangana, 2020). Therefore, the use of those non-Darcian flow functions, regardless of the Forchheimer and Izbash functions, should be regarded as a phenomenological approximation based on the measured relationship between the hydraulic gradient and the specific discharge. In another word, trying to find an exact hydrogeological interpretation of such non-Darcian flow equation is still debatable and requires much more new research. One should be aware that such functions may only be valid within a certain range of the hydraulic gradient (or specific discharge).

Secondly, the Izbash equation is a powerful analytical tool for analyzing the non-Darcian flow (Feng and Wen, 2016; Li et al., 2021; Qian et al., 2018; Wen et al., 2016; Zhu and Wen, 2020) but it has also been criticized for not satisfying the two extremes as the Forchheimer

equation, i.e., it does not automatically degenerate to Darcy's law when the specific discharge is sufficiently small or degenerate to the fully turbulent flow when the specific discharge is sufficiently large. However, it is worthwhile to point out that use of the Izbash equation is not focused on those two extremes, instead, it is more focused on the intermediate range of the specific discharge, which may be better described with a power-law function for some field circumstances. This is exactly the case for the field site investigated in this study. The reason for the Izbash equation to work satisfactorily for this field site is not completely clear, but we can speculate that it has something to do with the specific fracture networks at the field site of concern. Once again, trying to make a direct hydrogeological interpretation of the parameters used in the power-law function for a specific field site will be challenging and requires further research. Based on above discussion, the Izbash equation will be considered here to depict the non-Darcian flow in the fractured media to build a mathematical model in a double-porosity framework for parameter estimation.

The aquifer is supposed to be horizontal, confined with a thickness of b [L], and extends to infinity laterally. The hydraulic properties are assumed to be homogeneous and horizontally isotropic in each continuum with both fractured system and matrix system (Fig. 5). As the pumping well (W1) is fully penetrating, so vertical flow is not a concern in this study. For the fractured continuum, the governing equation of flow is:

$$\frac{\partial q(r, t)}{\partial r} + \frac{q(r, t)}{r} = \frac{S_f}{b} \frac{\partial s_f(r, t)}{\partial t} + q_a \quad (1)$$

where $q(r, t)$ is the specific discharge [L/T]; S_f is the storage coefficient of the fracture [-]; $s_f(r, t)$ represent the drawdown of the fracture [L]; q_a is the fluid exchange between fracture and matrix [L/T]; b is the thickness of aquifer [L]; t is time [T]; r is the radial distance from the well [L].

In a general double-permeability framework, the groundwater flow in rock matrix is Darcian and can be governed by the following equation (Barenblatt et al., 1960, De Smedt, 2011, Warren and Root, 1963):

$$K_m \nabla^2 s_m(r, t) = \frac{S_m}{b} \frac{\partial s_m(r, t)}{\partial t} - q_a \quad (2)$$

where K_m is the hydraulic conductivity of the matrix [L/T]; $s_m(r, t)$ represents the drawdown of the matrix [L]; S_m is the storage coefficient of the matrix [-]. It is important to notice that with the double-porosity framework (which is a subset of the double-permeability framework), the rock matrix permeability K_m is assumed to be extremely small and negligible, thus the left-hand side of Eq. (2) is essentially zero (De Smedt, 2011, Moench, 1984, Warren and Root, 1963). The fluid exchange q_a between fracture and matrix under the assumption of pseudo-steady state flow is governed by the following equation (De Smedt, 2011).

$$q_a = \alpha K_m [s_f(r, t) - s_m(r, t)] \quad (3)$$

where α is a shape factor with a dimension of inverse area [L⁻²], and it is related to the geometry of the matrix elements and controls the flow exchange between the fracture and matrix.

The assumption of the left side of Eq. (2) to be zero yields the expression for q_a , which is substituted into Eqs. (1) and (3), then one has

$$\frac{\partial q(r, t)}{\partial r} + \frac{q(r, t)}{r} = \frac{S_f}{b} \frac{\partial s_f(r, t)}{\partial t} + \frac{S_m}{b} \frac{\partial s_m(r, t)}{\partial t} \quad (4)$$

and

$$S_m \frac{\partial s_m(r, t)}{\partial t} = C [s_f(r, t) - s_m(r, t)] \quad (5)$$

respectively, where $C = \alpha K_m b$ is the leakage coefficient between fractures and matrix [T⁻¹].

Initial drawdowns in the fractures and the matrix are zero everywhere

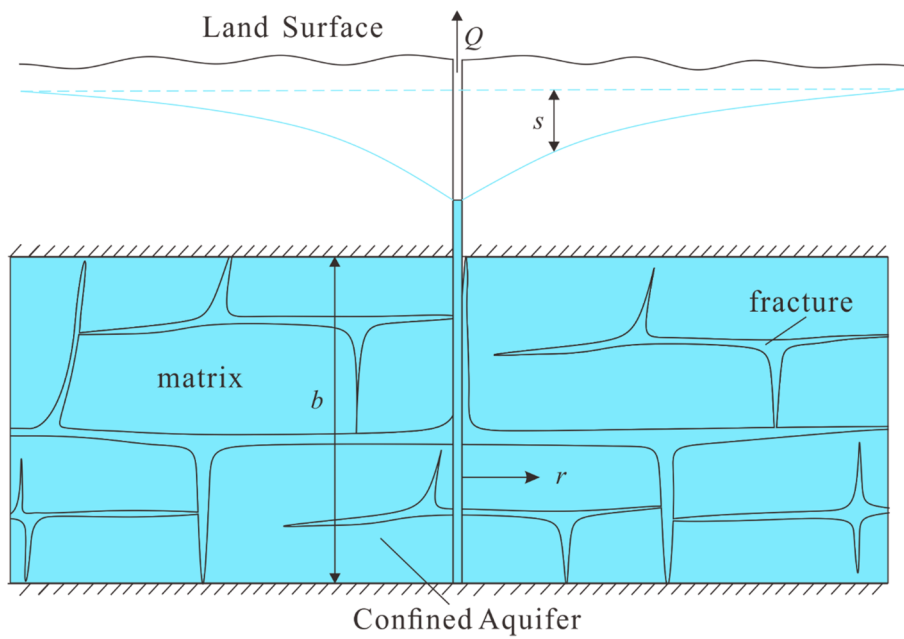


Fig. 5. The schematic diagram of the confined aquifer with double-porosity.

$$s_f(r, 0) = s_m(r, 0) = 0 \quad (6)$$

The outer boundary conditions far away from the pumping well are described as

$$s_f(\infty, t) = s_m(\infty, t) = 0 \quad (7)$$

And for a well radius approaching zero, one has

$$\lim_{r \rightarrow 0} 2\pi r b q(r, t) = -Q \quad (8)$$

with Q as the pumping rate [L^3/T], which is positive for pumping and negative for injection.

Applying the Izbash equation to describe the non-Darcian flow (Wen et al., 2008a), one has

$$[q(r, t)]^n = K_q \frac{\partial s_f(r, t)}{\partial r} \quad (9)$$

in which K_q and n are constants, the value of n is between 1 and 2 and K_q is termed the quasi hydraulic conductivity [$(\text{L}/\text{T})^n$]. When n equals to 1, Eq. (9) turns to Darcy's law and K_q becomes the hydraulic conductivity. Eq. (9) can be rewritten as

$$q(r, t) = K_q^{\frac{1}{n}} \left[\frac{\partial s_f(r, t)}{\partial r} \right]^{\frac{1}{n}} \quad (10)$$

Substituting Eq. (10) into Eq. (4) will yield:

$$\frac{\partial^2 s_f}{\partial r^2} + \frac{n}{r} \frac{\partial s_f}{\partial r} = \frac{S_f}{b} \frac{n}{K_q^{\frac{1}{n}}} \left(\frac{\partial s_f}{\partial r} \right)^{\frac{n-1}{n}} \frac{\partial s_f}{\partial t} + \frac{S_m}{b} \frac{n}{K_q^{\frac{1}{n}}} \left(\frac{\partial s_f}{\partial r} \right)^{\frac{n-1}{n}} \frac{\partial s_m}{\partial t} \quad (11)$$

Eq. (11) is a nonlinear governing equation. Using a time-independent approximation term to replace $\partial s_f/\partial r$ on the right side of Eq. (11) as follows (Wen et al., 2008a)

$$\frac{\partial s_f(r, t)}{\partial r} = \frac{[q(r, t)]^n}{K_q} \approx -\frac{\left(\frac{Q}{2\pi r b} \right)^n}{K_q} \quad (12)$$

Approximation of Eq. (12) has been extensively discussed before (Wen et al., 2008b) and will not repeat here. After considering Eq. (12), Eq. (11) then turns into

$$\frac{\partial^2 s_f}{\partial r^2} + \frac{n}{r} \frac{\partial s_f}{\partial r} = \frac{S_f}{b} \frac{n}{K_q} \left(\frac{Q}{2\pi b} \right)^{n-1} r^{1-n} \frac{\partial s_f}{\partial t} + \frac{S_m}{b} \frac{n}{K_q} \left(\frac{Q}{2\pi b} \right)^{n-1} r^{1-n} \frac{\partial s_m}{\partial t} \quad (13)$$

The solution of Eqs. (5) and (13) can be obtained by means of the Laplace transform (the detailed derivation process is in Appendix A) (De Smedt, 2011, Wen et al., 2008a). Finally, the solution of the drawdown in Laplace domain for fracture flow is

$$\bar{s}_f(r, p) = \frac{2 \left(\frac{Q}{2\pi b} \right)^n \left(\frac{1}{3-n} \sqrt{Ap + Bp \frac{C}{pS_m + C}} \right)^{\frac{2}{3-n}}}{K_q p \sqrt{Ap + Bp \frac{C}{pS_m + C}} \Gamma \left(\frac{2}{3-n} \right)} r^{\frac{1-n}{2}} K_{\frac{1-n}{3-n}} \left(\frac{2}{3-n} r^{\frac{3-n}{2}} \sqrt{Ap + Bp \frac{C}{pS_m + C}} \right) \quad (14)$$

where $K_{\frac{1-n}{3-n}}(x)$ is the modified Bessel function of the second kind and $\frac{1-n}{3-n}$ is the order, Γ is the gamma function, p is the Laplace transform parameter in respect to time, and over bar represents the term in Laplace domain. When the storage coefficient in matrix (S_m) goes to zero, B equals to zero, or the fluid exchange between fractures and the matrix C goes to zero, then Eq. (14) reduces to the single-porosity flow (Wen et al., 2008a).

$$\bar{s}_f(r, p) = \frac{2 \left(\frac{Q}{2\pi b} \right)^n \left(\frac{\sqrt{Ap}}{3-n} \right)^{\frac{2}{3-n}}}{K_q p \sqrt{Ap} \Gamma \left(\frac{2}{3-n} \right)} r^{\frac{1-n}{2}} K_{\frac{1-n}{3-n}} \left(\frac{2}{3-n} r^{\frac{3-n}{2}} \sqrt{Ap} \right) \quad (15)$$

When n goes to one, $\Gamma(1) = 1$, the flow is Darcian, and Eq. (14) changes to the solution of Darcian flow in a dual-porosity system (De Smedt, 2011, Moench, 1984, Warren and Root, 1963),

$$\bar{s}_f(r, p) = \frac{Q}{2\pi T p} K_0 \left(r \sqrt{\frac{pS_f}{T} + \frac{pCS_m}{T(pS_m + C)}} \right) \quad (16)$$

where $T = K_b$ is the overall aquifer transmissivity [L^2T^{-1}].

To obtain the real time solution, one needs to conduct the inverse Laplace transform to Eq. (14). Among several different candidates of inverse Laplace transform techniques such as Stehfest method (Stehfest, 1970, 1970b), Talbot method (Talbot, 1979), Weeks method (Weeks,

1966) and de Hoog method (De Hoog et al., 1982), and many others (Kuhlman, 2012, Wang et al., 2017, Zhan et al., 2009), the Stehfest method is straightforward to use with sufficient accuracy. Particularly, the Stehfest method in this study has used a 16-term ($N = 16$) series approximation.

2.4. Dimensionless transformation

Dimensionless terms are adopted here for parameter analysis to eliminating the effect of unit system and to reduce the number of free parameters. Defining the dimensionless variables in Table 1, Eqs. (4)–(8) can be transformed accordingly as follows:

$$\frac{\partial q_D}{\partial r_D} + \frac{q_D}{r_D} = -\frac{\partial s_{fD}}{\partial t_D} - \frac{\partial s_{mD}}{\partial t_D} \quad (17)$$

$$\phi \frac{\partial s_{mD}}{\partial t_D} = C_D (s_{fD} - s_{mD}) \quad (18)$$

$$s_{fD}(r_D, 0) = s_{mD}(r_D, 0) = 0 \quad (19)$$

$$s_{fD}(\infty, t_D) = s_{mD}(\infty, t_D) = 0 \quad (20)$$

$$\lim_{r_D \rightarrow 0} \frac{1}{2} r_D q_D = 1 \quad (21)$$

where the subscript D denotes the dimensionless terms hereinafter; ϕ is the storage ratio, dimensionless.

The Izbash equation Eq. (9) is also transformed in dimensionless format as

$$(q_D)^n = K_{qD} \frac{\partial s_{fD}}{\partial r_D} \text{ or } q_D = K_{qD}^{1/n} \left(-\frac{\partial s_{fD}}{\partial r_D} \right)^{1/n}, \quad (22)$$

$$\frac{\partial^2 s_{fD}}{\partial r_D^2} + \frac{n}{r_D} \frac{\partial s_{fD}}{\partial r_D} = \frac{n}{K_{qD}^{1/n}} \left(-\frac{\partial s_{fD}}{\partial r_D} \right)^{\frac{n-1}{n}} \frac{\partial s_{fD}}{\partial t_D} + \frac{\phi n}{K_{qD}^{1/n}} \left(-\frac{\partial s_{fD}}{\partial r_D} \right)^{\frac{n-1}{n}} \frac{\partial s_{mD}}{\partial t_D} \quad (23)$$

The non-linear term $\left(-\frac{\partial s_{fD}}{\partial r_D} \right)^{\frac{n-1}{n}}$ in Eq. (23) can be eliminated by the linearization procedure. Using the condition that flow rates passing through any closed interfaces surrounding the well are equal to the pumping rate Q at the steady-state, the approximate of the specific discharge at any time can be defined as

$$\frac{1}{2} r_D q_D \approx 1 \quad (24)$$

With Eqs. (22) and (24), the non-linear term can be rewritten as

$$\left(-\frac{\partial s_{fD}}{\partial r_D} \right)^{\frac{n-1}{n}} \approx \left(\frac{2}{r_D K_{qD}^{1/n}} \right)^{n-1} \quad (25)$$

Substituting Eq. (25) to Eq. (23) results in

$$\frac{\partial^2 s_{fD}}{\partial r_D^2} + \frac{n}{r_D} \frac{\partial s_{fD}}{\partial r_D} = A_D r_D^{1-n} \frac{\partial s_{fD}}{\partial t_D} + B_D r_D^{1-n} \frac{\partial s_{mD}}{\partial t_D} \quad (26)$$

$$\text{where } A_D = \frac{n}{2^{1-n} K_{qD}}, B_D = \frac{\phi n}{2^{1-n} K_{qD}}.$$

The inner boundary condition near the well in dimensionless format can be expressed as

$$\frac{1}{2} r_D q_D \Big|_{r_D \rightarrow 0} = 1 \quad (27)$$

The details of solving Eq. (26) by the Laplace transform are similar to the procedure of solving the dimensional format of equation groups and the details can be found in Appendix A. With the boundary Eq. (27), the solution for Eq. (26) in the Laplace domain is now expressed as

$$\overline{s_{fD}}(r_D, p_D) = \frac{2^{n+1} \left(\frac{1}{3-n} \sqrt{A_D p_D + B_D p_D \frac{C_D}{\phi p_D + C_D}} \right)^{\frac{2}{3-n}}}{K_{qD} p_D \sqrt{A_D p_D + B_D p_D \frac{C_D}{\phi p_D + C_D}} \Gamma\left(\frac{2}{3-n}\right)} r_D^{\frac{1-n}{2}} K_{\frac{1-n}{2}} \left(\frac{2}{3-n} r_D^{\frac{3-n}{2}} \sqrt{A_D p_D + B_D p_D \frac{C_D}{\phi p_D + C_D}} \right), \quad (28)$$

where K_{qD} can be regarded as a dimensionless apparent conductivity. Note that the minus sign must be included in the bracket to make q_D positive.

With the substitution of Eq. (22) into Eq. (17), one has

where p_D is the Laplace transform variable in respect to the dimensionless time t_D , overbar means the term in Laplace domain, $\overline{s_{fD}}(r_D, p_D)$ is the dimensionless drawdown in the Laplace domain, $K_\nu(x)$ is the second kind ν -order modified Bessel functions, where $\nu = (1 - n)/(3 - n)$, $\Gamma(x)$ is the gamma function.

3. Results and discussion

3.1. Analysis of parameters

The drawdown response in the fracture to pumping can be approximately classified to three stages (i.e., early-, intermediate-, and late-time stages). At the early time, the fracture responses to the pumping immediately after the start of pumping, but the matrix has not responded to pumping yet because the water exchange between the matrix and the fracture is rate-limited and requires time. During this stage, the system functions as a single-porosity (fracture) media. At the late stage, the matrix and the fracture have reached a hydrodynamic equilibrium, thus the drawdown in the matrix is the same as the drawdown in the fracture at any given location, and the water exchange between the matrix and the fracture also ceases because there is no hydraulic head

Table 1
Definition of the dimensionless variables.

$r_D = r/b$	$q_D = -\frac{4\pi b^2 q}{Q}$
$t_D =$	$s_{mD} = \frac{4\pi b K_q^{1/n}}{Q} s_m$
$\frac{1}{n} t$	
$\frac{K_q}{S_f b}$	$s_{fD} = \frac{4\pi b K_q^{1/n}}{Q} s_f$
$C_D =$	$K_{qD} = \left(\frac{4\pi b^2 K_q^{1/n}}{Q} \right)^{n-1}$
$\frac{C_D}{K_q}$	

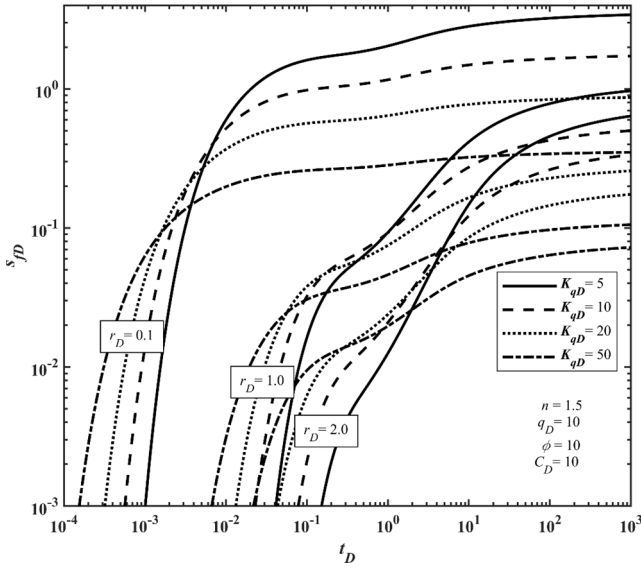


Fig. 6. Dimensionless drawdown versus dimensionless time with $n = 1.5$, $q_D = 10$ and $C_D = 10$ for the values of dimensionless quasi-conductivity $K_q = 5, 10, 20, 50$ and $r_D = 0.1, 1.0$ and 2.0 , respectively.

difference between the matrix and the fracture to drive water flow between them. During this stage, the system also functions as a single-porosity media but with an augmented porosity equaling the summation of porosities of the matrix and the fracture. At the late stage, the fracture acts as a conducting medium while the matrix is the main source of supply for pumping. At the intermediate stage, however, the water exchange between the matrix and the fracture plays an important role in regulating the drawdown in the fracture, and a greater water exchange rate (i.e., a larger C_D) means a greater contribution of the matrix storage to the fracture, thus will lead to a smaller drawdown in the fracture. The parameter analysis of the drawdown behaviors will be specifically illustrated as follows.

The analysis of the dimensionless non-Darcian conductivity K_{qD} , which is an important parameter to describe the characteristic of the aquifer, is shown in Fig. 6. A larger non-Darcian conductivity K_{qD} represents a greater capability for the fracture to transmit water to the

pumping well, thus, a quicker response to pumping will be observed in the fracture at the early state of pumping, as evident in Fig. 6. At the late stage, however, a greater K_{qD} means that a smaller hydraulic gradient is required to transmit the same amount of water to the pumping well, thus the drawdown curve looks flatter, and the drawdown is also smaller for a greater K_{qD} .

The dimensionless parameter $\phi = S_m/S_f$ represents the distinction of water storage capacity of fracture and matrix, which is analyzed in Fig. 7. A larger ϕ represents a larger storativity difference between the matrix and the fracture. In another word, a larger ϕ means a greater replenishment capacity from the rock matrix to the fracture, thus will lead to a smaller drawdown in the fracture. Furthermore, a larger ϕ also implies a greater volume of matrix storage, thus will lead to a longer transitional period of water exchange between the matrix and the fracture. When ϕ equals to zero, which essentially reduces the double-porosity media to the single-porosity fracture media (or the storage coefficient of matrix is inexistence), the drawdown curves are simplified to those of non-Darcian flow in a single-porosity system, as expected.

The dimensionless leakage coefficient C_D between the matrix and the fracture is a lumped parameter which is related to the conductivity of matrix and the characteristic of fluid exchange between matrix and fracture. This parameter is responsible for water exchange rate between matrix to fracture, thus can affect the overall behavior of drawdown characteristics. As Fig. 8 shows, the fracture drawdown curves are similar at the early and late stages for different values of C_D in a non-Darcian double-porosity system, while the drawdown in the transitional period is distinctly affected by the value of C_D , and a greater C_D means a smaller drawdown in the fracture at a given time. These observations are understandable. First, at the early pumping stage, the water exchange between the matrix and the fracture has not yet occurred as such an exchange process is rate-limited and requires time, thus the drawdown response in the fracture is not related to the value of C_D . At the late pumping stage, the matrix and the fracture has reached a hydrodynamic equilibrium, meaning that the drawdown in the matrix and the drawdown in the fracture has no difference from each other, thus the water exchange between the matrix and the fracture will cease (because such a water exchange term depends on the drawdown difference between the matrix and the fracture). Therefore, the drawdown response at the late stage will not be related to the value of C_D . Second, during the intermediate pumping stage, the water exchange between the matrix and the fracture will play an important role and a greater C_D

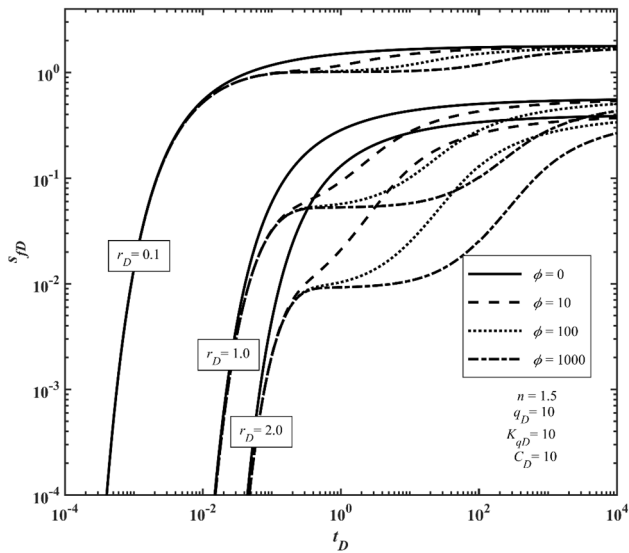


Fig. 7. Dimensionless drawdown versus dimensionless time with $n = 1.5$, $q_D = 10$, $K_q = 5$, and $C_D = 10$ for the storage ratio $\phi = 0, 10, 100, 1000$ and $r_D = 0.1, 1.0$ and 2.0 , respectively.

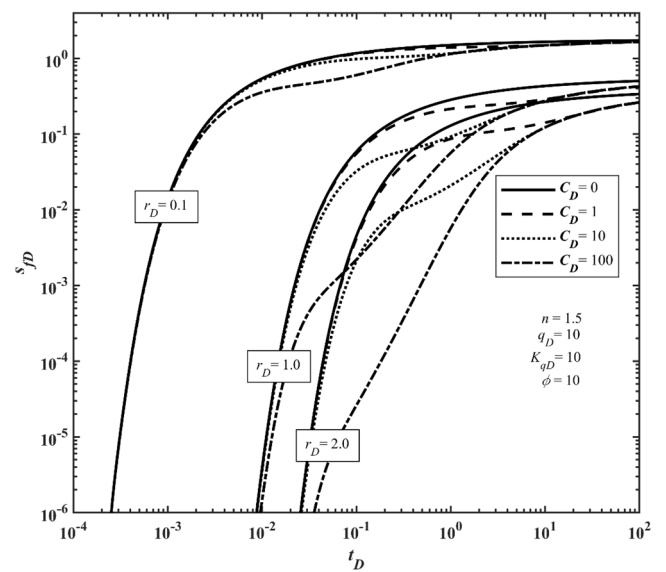


Fig. 8. Drawdown versus time with $n = 1.5$, $q_D = 10$, $K_q = 5$, and $\phi = 10$ for the dimensionless leakage coefficient $C_D = 0, 1, 10, 100$ and $r_D = 0.1, 1.0$ and 2.0 , respectively.

Table 2

Calculated hydraulic parameters for this study and other reference models.

Well	W2	W3	W4	W5
r (m)	5.57	54.84	73.48	81.91
This study	1.08	1.064	1.09	1.096
n	1.00×10^{-5}	1.18×10^{-5}	6.59×10^{-6}	6.57×10^{-6}
K_q (m/s) ⁿ	5.00×10^{-2}	3.93×10^{-4}	6.62×10^{-4}	4.76×10^{-4}
S_f	4.04×10^{-1}	8.71×10^{-3}	4.65×10^{-3}	4.18×10^{-3}
ϕS_f				
C (s ⁻¹)	1.87×10^{-4}	8.97×10^{-6}	4.67×10^{-6}	5.04×10^{-6}
K (m/s)	3.98×10^{-5}	1.42×10^{-5}	7.43×10^{-6}	7.20×10^{-6}
S	6.53×10^{-2}	4.33×10^{-3}	4.50×10^{-3}	2.67×10^{-3}
σS	2.85×10^{-1}	6.08×10^{-2}	7.91×10^{-2}	8.55×10^{-2}
λ	8.87×10^{-3}	3.20×10^{-3}	7.88×10^{-4}	5.70×10^{-5}
K (m/s)	2.67×10^{-5}	5.51×10^{-5}	5.02×10^{-5}	3.94×10^{-5}
S_f	7.13×10^{-2}	1.82×10^{-3}	9.96×10^{-4}	2.80×10^{-4}
ϕS_f	4.50×10^{-1}	3.01×10^{-3}	2.56×10^{-3}	3.37×10^{-3}
C (s ⁻¹)	1.33×10^{-4}	4.19×10^{-5}	1.23×10^{-5}	5.87×10^{-5}
n	1.04	1.05	1.036	1.03
K_q (m/s)	1.70×10^{-5}	1.60×10^{-5}	1.28×10^{-5}	1.25×10^{-5}
S	2.54×10^{-4}	8.40×10^{-6}	6.68×10^{-6}	6.69×10^{-6}

means a greater rate of supply of water from the matrix storage to the fracture, thus will lead to a smaller drawdown in the fracture. Above observations will also occur when flow in the fracture continuum is strictly Darcian. Occurrence of non-Darcian flow in the fracture continuum will modify the actual values of drawdown but generally will not change the overall pattern of the type curves.

3.2. Parameter inversion and discussion

To put the above theory into application, we will employ the solutions to interpret the pumping test described in Section 2. For the purpose of comparison, we will also use the Liu solution (single-porosity with non-Darcian flow) and the Warren and Root / De Smedt solution (double-porosity with Darcian flow) to interpret the same set of data and to compare the results of parameter estimated using such different interpretative theories. It is notable that there is a minor difference between the model of Warren and Root (1963) and the model of De Smedt (2011). The storage ratio σ in the Warren and Root model refers to the total storage of fracture and matrix combined with respect to the storage of fracture S_f , yet the De Smedt solution is expressed as the storage of matrix S_m with respect to the storage of fracture S_f (which is the same as the definition of storage ratio in this study), considering the

delayed response of the matrix to the pumping test. Here, a particle swarm optimization (PSO) algorithm has been introduced to a self-written MATLAB source code to get the optimal hydrogeological parameters, and the effectiveness of the PSO algorithm has been proven in a number of recent studies such as (Chen et al., 2020). The advantage of PSO algorithm is that the particle has 'memory', which can update itself by tracking the extreme value in each iteration, and eventually find the optimal solution of multi-parameter group quickly and efficiently. In the case of different populations size ($N_p = 40, 80$ and 120), the results of estimated aquifer parameters are very close to each other, among which the result of a population size of $N_p = 40$ is the most appropriate. Therefore, $N_p = 40$ is used in the PSO algorithm in this study.

Table 2 shows the hydraulic parameters obtained by matching the four theoretical type curves with observed drawdown data. Here, the calculated hydraulic parameters are used to predict the recovery curve during recovery period and are plotted in the same picture with the drawdown in pumping time, as shown in Figs. 9 to 12. Several interesting observations can be made from these figures.

First, it is clearly evident that the curves of the non-Darcian double-porosity model of this study provide better fit with the pumping and recovery data than the other three reference solutions of Liu et al. (2016), Warren and Root (1963) and De Smedt (2011). We need to point

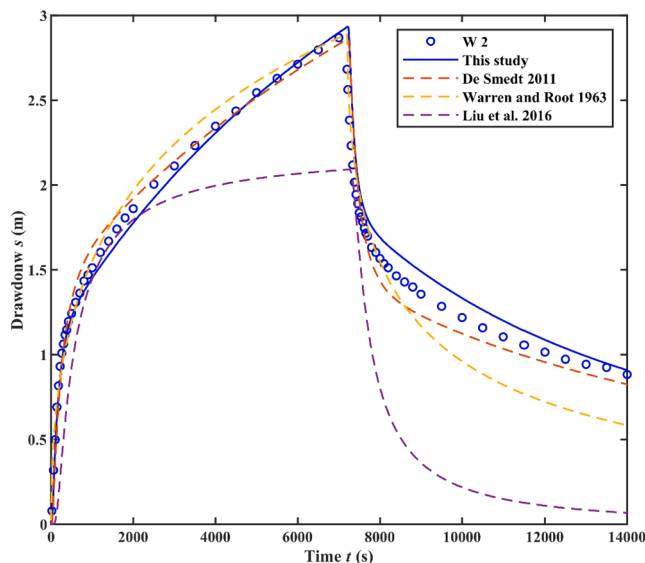


Fig. 9. Comparation of the W2 observed drawdowns with calculated drawdown based on Warren and Root (1963) model, De Smedt (2011) model, Liu et al. (2016) and non-Darcian dual-porosity model of this study.

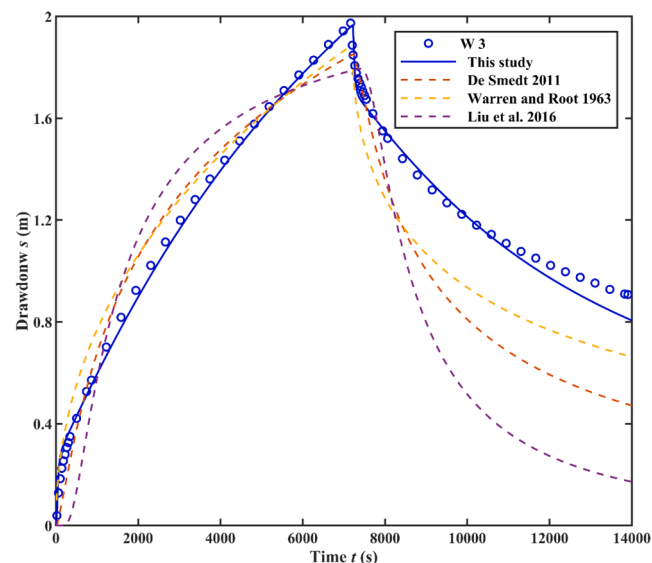


Fig. 10. Comparation of the W3 observed drawdowns with calculated drawdown based on Warren and Root (1963) model, De Smedt (2011) model, Liu et al. (2016) and non-Darcian dual-porosity model of this study.

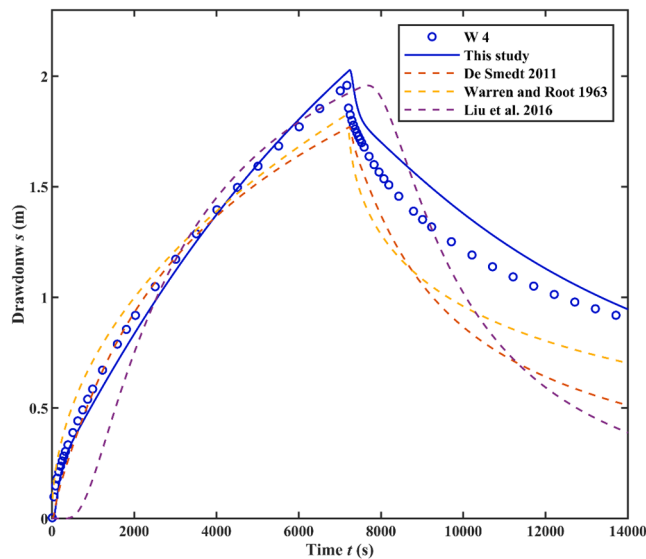


Fig. 11. Comparation of the W4 observed drawdowns with calculated drawdown based on Warren and Root (1963) model, De Smedt (2011) model, Liu et al. (2016) and non-Darcian dual-porosity model of this study.

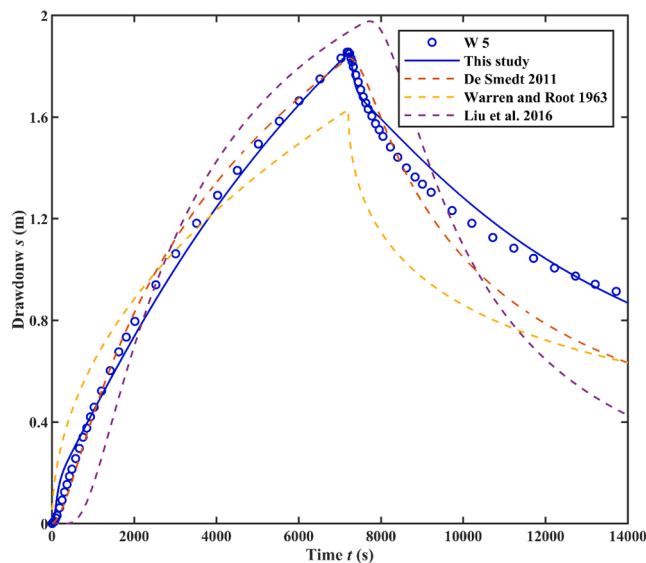


Fig. 12. Comparation of the W5 observed drawdowns with calculated drawdown based on Warren and Root (1963) model, De Smedt (2011) model, Liu et al. (2016) and non-Darcian dual-porosity model of this study.

out that a better fit between a model and field data should not be used as the only criterion of warranting a model's superiority as a model involving more fitting parameters usually will do a better job in curve fitting, but such best-fitting exercises can provide some insurance of a model's suitability and further evidence is required to validate a model's applicability. Second, the single-porosity model of Liu et al. (2016) is clearly incapable of reproducing the pumping and recovery data, showing that double-porosity nature of the heterogeneous media must be considered. The Darcian flow double-porosity models of Warren and Root (1963) and De Smedt (2011) provide better fitting than the single-porosity model of Liu et al. (2016) but they appear to overestimate the drawdown during the intermediate time of pumping and significantly underestimate the residual drawdown during most time of the recovery stage. Furthermore, the fitting of the double-porosity models of Warren and Root (1963) and De Smedt (2011) during the recovery period is very poor, suggesting that some additional mechanisms of flow are probably

missing in those models to explain the field data. Third, our model of this study provides substantial improvement in terms of fitting than the other three models, but in general the fitting during the recovery period is worse than the fitting during the pumping period. Specifically, we notice that our model appears to mildly overestimate the residual drawdown during the recovery period for well W4, although the fittings for the other three wells W2, W3, and W5 are better during the recovery period.

Some of above observations may be understood from a hydrodynamic standpoint. For instance, let us compare the hydrodynamic characteristics of this model (non-Darcian double-porosity flow) and those of Warren and Root (1963) and De Smedt (2011) (Darcian double-porosity flow) during the intermediate pumping stage. Comparing with the Darcian flow model which only considers viscous flow, the non-Darcian flow model considers the inertial flow effect in addition to the viscous flow component. Therefore, when the pumping starts and the cone of depression begins to expand rapidly from the pumping well, the inertial effect in the fracture continuum in the non-Darcian double-porosity model means additional resistance to flow or greater energy loss (or greater hydraulic head loss) to flow during this early stage of pumping as compared to the Darcian double-porosity models. Such a greater hydraulic head loss in the fracture continuum (during the early stage of pumping) will create a greater hydraulic head difference between the fracture continuum and matrix continuum, which will lead to a greater water flow rate from the matrix continuum to the fracture continuum at the intermediate stage of pumping. Because of the greater contribution of water flux from the matrix continuum to the fracture continuum during the intermediate stage, the fracture continuum will experience less drawdown.

For the recovery period, different hydrodynamic characteristics of the non-Darcian double-porosity model and the Darcian double-porosity model may also explain the observations made above from Figs. 9–12. For instance, at the moment of recovery (or the end of pumping), the cone of depression has already expanded to its maximum with a large influenced volume of fractured media surrounding the pumping well. At this moment, the inertial effect of the non-Darcian double-porosity flow model can be significant. When pumping stops (or recovery starts), the hydraulic head starts to rise. However, because of the inertial effect of the non-Darcian flow, it is more difficult to recover the drawdown in the non-Darcian double-porosity model as compared to the Darcian double-porosity model (which does not include the inertial effect). In another word, the residual drawdown in the non-Darcian double-porosity model is higher than that in the Darcian double-porosity model, which is clearly visible in Figs. 9–12. In fact, the significant improvement of this model as compared to the Darcian double-porosity models of Warren and Root (1963) and De Smedt (2011) leads us to believe that one must consider the non-Darcian nature of flow in the media. The minor discrepancy of this model and the field test data during the recovery period may also suggest that even with the consideration of the non-Darcian flow, the actual flow field is probably even more complex than the simplified two-parameter Izbash equation. This is a subject we will continue to investigate in the future.

As is shown in Table 2, the calculated quasi hydraulic conductivity (K_q) for the fracture continuum range from 6.57×10^{-6} (m/s)ⁿ to 1.18×10^{-5} (m/s)ⁿ, while the hydraulic conductivity values of the fracture continuum obtained from the other two double-porosity models are 7.2×10^{-6} m/s – 3.98×10^{-5} m/s for Warren and Root (1963) and 2.67×10^{-5} m/s – 5.51×10^{-5} m/s for De Smedt (2011). Although it is not very meaningful to rigorously compare the quasi hydraulic conductivity of the non-Darcian flow with the hydraulic conductivity as they are not exactly the same parameter and have different units as well, one can still see that the variational range of the quasi hydraulic conductivity of our model here (which is 5.23×10^{-6} (m/s)ⁿ) is about one order of magnitude smaller than those of the hydraulic conductivity obtained from the Darcian double-porosity models (which are 3.26×10^{-5} m/s for Warren and Root (1963) and 3.84×10^{-5} m/s for De Smedt (2011)).

The narrower range of the fitted parameter in some degree suggests that including the non-Darcian flow into the double-porosity model is a reasonable approach than the double-porosity model excluding the non-Darcian flow. The fitted storativity of the fracture medium (S_f) ranges from 4.76×10^{-4} to 5.0×10^{-2} using the new model of this study. This value is somewhat similar to the values obtained using the Warren and Root (1963) model (2.67×10^{-3} - 6.53×10^{-2}) and the De Smedt (2011) model (2.80×10^{-4} - 7.13×10^{-2}).

3.3. Discussion

Although the non-Darcian double-porosity model appears to work better than the non-Darcian single-porosity model (i.e., the Liu's model) and the Darcian double-porosity model (i.e., the Warren and Root's model or De Smedt's model) for interpreting the pumping test results of this study, some factors have not been taken into account and further investigations are probably needed in the future.

Firstly, some complexities that are likely associated with many pumping tests have not been included in this investigation. For instance, the wellbore storage (Wen et al., 2006, Zhu and Wen, 2020), skin effect (Chen et al., 2020) and the effect of variation in pumping rate have not been considered. The wellbore storage effect may be secondary as the radius of the pumping well used in this study is relatively small ($r_w = 0.115$ m), but the impact of skin effect is unknown due to lack of information. Secondly, the Izbash equation used in this study appears to be satisfactory, but a comprehensive comparison study of the proposed model with other possible alternative models has not been reported here, due to the limit of scope of this investigation. This is based on a few considerations. First of all, the Izbash equation, despite of its empirical nature, appears to work very well for interpreting the pumping test data here. This equation works particularly well in the near field where the non-Darcian flow effect is most profound, which happens to be the focus of this investigation. Wu (2002) has used Forchheimer equation to obtain the steady-state solution of non-Darcian flow in a double-porosity framework, but such a steady-state solution cannot be used for interpreting transient pumping test data. In the future, it is necessary to work with the Forchheimer type of non-Darcian flow in a double-porosity framework under transient flow condition. Thirdly, it should also be worthwhile to develop non-Darcian flow in a double-permeability framework in the future if the matrix-to-matrix flow (without through the fracture network) becomes non-negligible. Fourthly, this research is based on the presumption that the fractured media can be conceptualized as two homogeneous continuums: the fracture network continuum and rock matrix continuum. Such a presumption of course is idealized because it essentially assumes that the fracture network does not have any heterogeneity or preference of orientations. The homogeneity presumption may be questionable as some realistic fracture networks could be heterogeneous and may have preferred orientations.

4. Conclusions

An analytical solution is presented for describing radial flow in double-porosity fractured aquifers by considering non-Darcian flow in fracture continuum. The behavior of drawdown with time in the frac-

tured continuum is characterized by five parameters: n , K_q , C , S_m and S_f . The special case of our solution when n equals to 1 is the same as the De Smedt (2011) solution that assume Darcian flow in the fracture continuum. Another special case of our solution for C or S_m equaling to zero turns to Wen (2008a) solution for single-porosity aquifers. A dimensionless solution is derived for parameter sensitivity analysis. A larger dimensionless non-Darcian conductivity K_{qD} value means a larger drawdown in early pumping time, while a smaller drawdown in late pumping time. A larger C_D or ϕ value promotes greater water exchange between fracture continuum and matrix continuum, causing a more profound (and longer) transitional stage.

The Darcian double-porosity models of Warren and Root (1963) and De Smedt (2011) overestimate the drawdown in the intermediate time during the pumping period while significantly underestimate the residual drawdown during the recovery period without considering the non-Darcian flow in fracture. In addition, the non-Darcian single-porosity model of Liu et al. (2016) performs poorly to match the field data for both the pumping period and recovery period.

The proposed new model considering non-Darcian flow using an empirical power-law based (Izbash) equation in a double-porosity framework has successfully explained the observed drawdown type curves and derivative drawdown type curves as well. The new model has been successfully applied for estimating aquifer parameters such as hydraulic conductivity (or quasi hydraulic conductivity) and storage capacities using a particle swarm optimization (PSO) algorithm.

The research is limited for not considering wellbore storage and skin effect and it relies on the promise that the media can be conceptualized as two interrelated homogenous continuums (fracture network and rock matrix). It also depends on the suitability of a power-law based non-Darcian flow equation to derive the (semi)-analytical solutions presented.

CRediT authorship contribution statement

Yilin Wang: Conceptualization, Data curation, Writing - original draft. **Hongbin Zhan:** Methodology, Validation, Writing - review & editing. **Kun Huang:** Conceptualization, Methodology. **Linqing He:** Investigation. **Junwei Wan:** Funding acquisition, Investigation, Writing - review & editing.

Declaration of Competing Interest

The authors declare that they have no known competing financial interests or personal relationships that could have appeared to influence the work reported in this paper.

Acknowledgement

This study was partially supported by the Hunan Exploration Design Institute. The authors would like to express their immense gratitude to the editors for offering us valuable suggestions, which significantly helped improve the quality of the manuscript. Sincere thanks to all the anonymous reviewers for their detailed comments and crucial observations.

Appendix A. Semi-analytical solution of non-Darcian double-porosity model in Laplace domain

The solution of Eqs. (5) and (13) can be obtained by means of the Laplace transform (De Smedt, 2011, Wen et al., 2008a). Applying the Laplace transform to Eq. (5) leads to

$$pS_m\bar{s}_m = C(\bar{s}_f - \bar{s}_m) \quad (A1)$$

or

$$\bar{s}_m = C\bar{s}_f / (pS_m + C) \quad (A2)$$

where p is the Laplace transform parameter in respect to time, and the over bar denotes the terms in Laplace domain. Similarly, applying Laplace transform to Eq. (13) leads to

$$\frac{\partial^2 \bar{s}_f}{\partial r^2} + \frac{n}{r} \frac{\partial \bar{s}_f}{\partial r} = Ar^{1-n} p \bar{s}_f + Br^{1-n} p \bar{s}_m \quad (A3)$$

where $A = \frac{S_f}{b} \frac{n}{K_q} \left(\frac{\varrho}{2\pi b} \right)^{n-1}$, $B = \frac{S_m}{b} \frac{n}{K_q} \left(\frac{\varrho}{2\pi b} \right)^{n-1}$.

The boundary conditions in Laplace domain are transformed into

$$\bar{s}_f(\infty, p) = 0 \quad (A4)$$

$$\lim_{r \rightarrow 0} r^n \left(\frac{d \bar{s}_f}{dr} \right) = - \frac{\left(\frac{\varrho}{2\pi b} \right)^n}{K_q p} \quad (A5)$$

Substituting Eq. (A2) to Eq. (A3) to replace \bar{s}_m , one has

$$\frac{\partial^2 \bar{s}_f}{\partial r^2} + \frac{n}{r} \frac{\partial \bar{s}_f}{\partial r} = \left[Ap + Bp \frac{C}{(pS_m + C)} \right] r^{1-n} \bar{s}_f \quad (A6)$$

Eq. (A6) is a form of Bessel equation. The solution of Eq. (A6) can be written as

$$\bar{s}_f(r, p) = r^{\frac{1-n}{2}} \left[C_1 I_{\frac{1-n}{3-n}} \left(\frac{2}{3-n} r^{\frac{3-n}{2}} \sqrt{Ap + Bp \frac{C}{(pS_m + C)}} \right) + C_2 K_{\frac{1-n}{3-n}} \left(\frac{2}{3-n} r^{\frac{3-n}{2}} \sqrt{Ap + Bp \frac{C}{(pS_m + C)}} \right) \right] \quad (A7)$$

in which $I_{\frac{1-n}{3-n}}(x)$ and $K_{\frac{1-n}{3-n}}(x)$ are the first and second kinds of modified Bessel function with the order $\frac{1-n}{3-n}$, respectively; C_1 and C_2 are coefficients to be determined by the boundary conditions. Taking into account the boundary condition of Eq. (A4), one has $C_1 = 0$. Then, Eq. (A7) becomes

$$\bar{s}_f(r, p) = r^{\frac{1-n}{2}} \left[C_2 K_{\frac{1-n}{3-n}} \left(\frac{2}{3-n} r^{\frac{3-n}{2}} \sqrt{Ap + Bp \frac{C}{(pS_m + C)}} \right) \right] \quad (A8)$$

Applying Eq. (A5) in Eq. (A8) results in

$$C_2 r^n \left[\frac{1-n}{2} r^{\frac{-1-n}{2}} K_{\frac{1-n}{3-n}} \left(\frac{2}{3-n} r^{\frac{3-n}{2}} \sqrt{Ap + Bp \frac{C}{(pS_m + C)}} \right) + r^{\frac{1-n}{2}} K'_{\frac{1-n}{3-n}} \left(\frac{2}{3-n} r^{\frac{3-n}{2}} \sqrt{Ap + Bp \frac{C}{(pS_m + C)}} \right) r^{\frac{1-n}{2}} \sqrt{Ap + Bp \frac{C}{(pS_m + C)}} \right] = - \frac{\left(\frac{\varrho}{2\pi b} \right)^n}{K_q p} \quad (A9)$$

Recalling the following properties of the modified Bessel functions: $x dK_v(x)/dx + v K_v(x) = -x K_{v-1}(x)$ and $K_v(x) = K_{-v}(x)$, Eq. (A9) turns into

$$C_2 r^n \left[-r^{1-n} \sqrt{Ap + Bp \frac{C}{(pS_m + C)}} K_{\frac{2}{3-n}} \left(\frac{2}{3-n} r^{\frac{3-n}{2}} \sqrt{Ap + Bp \frac{C}{(pS_m + C)}} \right) \right] = - \frac{\left(\frac{\varrho}{2\pi b} \right)^n}{K_q p} \quad (A10)$$

Recalling that $K_v(x) \approx \frac{\Gamma(v)}{2} \left(\frac{x}{2} \right)^{-v}$, $v > 0$, when x goes to zero, in which $\Gamma()$ is the Gamma function, one can obtain

$$C_2 = \frac{2 \left(\frac{\varrho}{2\pi b} \right)^n \left(\frac{1}{3-n} \sqrt{Ap + Bp \frac{C}{(pS_m + C)}} \right)^{\frac{2}{3-n}}}{K_q p \sqrt{Ap + Bp \frac{C}{(pS_m + C)}} \Gamma \left(\frac{2}{3-n} \right)} \quad (A11)$$

Therefore, the solution of the drawdown in dual-porosity aquifer in Laplace domain is

$$\bar{s}_f(r, p) = \frac{2 \left(\frac{\varrho}{2\pi b} \right)^n \left(\frac{1}{3-n} \sqrt{Ap + Bp \frac{C}{(pS_m + C)}} \right)^{\frac{2}{3-n}}}{K_q p \sqrt{Ap + Bp \frac{C}{(pS_m + C)}} \Gamma \left(\frac{2}{3-n} \right)} - r^{\frac{1-n}{2}} K_{\frac{1-n}{3-n}} \left(\frac{2}{3-n} r^{\frac{3-n}{2}} \sqrt{Ap + Bp \frac{C}{(pS_m + C)}} \right) \quad (A12)$$

References

- Altinors, A., Onder, H., 2008. A double-porosity model for a fractured aquifer with non-Darcian flow in fractures. *Hydrol. Sci. J.* 53 (4), 868–882.
- Balhoff, M., Mikelic, A., Wheeler, M.F., 2009. Polynomial filtration laws for low Reynolds number flows through porous media. *Transp. Porous Media* 81 (1), 35–60.
- Banerjee, A., Pasupuleti, S., 2019. Effect of convergent boundaries on post laminar flow through porous media. *Powder Technol.* 342, 288–300.
- Banerjee, A., Pasupuleti, S., Singh, M.K., Kumar, G.N.P., 2017. A study on the Wilkins and Forchheimer equations used in coarse granular media flow. *Acta Geophys.* 66 (1), 81–91.
- Barenblatt, G.I., Zheltov, I.P., Kochina, I.N., 1960. Basic concepts in the theory of seepage of homogeneous liquids in fissured rocks [strata]. *J. Appl. Math. Mech.* 24 (5), 1286–1303.
- Blick, E.F., 1966. Capillary-orifice model for high-speed flow through porous media. *Ind. Eng. Chem. Process Des. Dev.* 5 (1), 90–94.
- Bolt, G.H., Groeneveld, P.H., 1969. Coupling phenomena as a possible cause of “Non-Darcian” behaviour of water in soil. *Int. Assoc. Sci. Hydrol. Bull.* 14 (2), 17–28.

- Bordier, C., Zimmer, D., 2000. Drainage equations and non-Darcian modelling in coarse porous media or geosynthetic materials. *J. Hydrol.* 228 (3-4), 174–187.
- Camac, B.A., Hunt, S.P., Boult, P.J., 2006. Local rotations in borehole breakouts—observed and modeled stress field rotations and their implications for the petroleum industry. *Int. J. Geomech.* 6 (6), 399–410.
- Chen, C., Wen, Z., Zhou, H., Jakada, H., 2020. New semi-analytical model for an exponentially decaying pumping rate with a finite-thickness skin in a leaky aquifer. *J. Hydrol. Eng.* 25 (8), 04020037. [https://doi.org/10.1061/\(ASCE\)HE.1943-5584.0001956](https://doi.org/10.1061/(ASCE)HE.1943-5584.0001956).
- Chen, Y.-F., Liu, M.-M., Hu, S.-H., Zhou, C.-B., 2015. Non-Darcy's law-based analytical models for data interpretation of high-pressure packer tests in fractured rocks. *Eng. Geol.* 199, 91–106.
- Cherubini, C., Giasi, C.I., Pastore, N., 2012. Bench scale laboratory tests to analyze non-linear flow in fractured media. *Hydrol. Earth Syst. Sci.* 16 (8), 2511–2522.
- Cherubini, C., Giasi, C.I., Pastore, N., 2013. Evidence of non-Darcy flow and non-Fickian transport in fractured media at laboratory scale. *Hydrol. Earth Syst. Sci.* 17 (7), 2599–2611.
- Cook, N.G.W., 1992. Natural joints in rock: mechanical, hydraulic and seismic behaviour and properties under normal stress. *Int. J. Rock Mech. Min. Sci. Geomech. Abstracts* 29 (3), 198–223.
- De Hoog, F.R., Knight, J.H., Stokes, A.N., 1982. An improved method for numerical inversion of laplace transforms. *Soc. Ind. Appl. Math.* 3 (3), 357–366.
- De Smedt, F., 2011. Analytical solution for constant-rate pumping test in fissured porous media with double-porosity behaviour. *Transp. Porous Media* 88 (3), 479–489.
- Ergun, S., 1952. Fluid flow through packed columns. *Chem. Eng. Prog.* 48, 89–94.
- Feng, Q., Wen, Z., 2016. Non-Darcian flow to a partially penetrating well in a confined aquifer with a finite-thickness skin. *Hydrogeol. J.* 24 (5), 1287–1296.
- Forchheimer, P.H., 1901. Wasserbewegung durch Boden [Movement of water through soil]. *Zeitschr. Ver. deutsch. Ing.*
- Hamm, S.-Y., Bidaux, P., 1996. Dual-porosity fractal models for transient flow analysis in fissured rocks. *Water Resour. Res.* 32 (9), 2733–2745.
- Izbash, S.V. (1931) O filtracii v kropnozernistom materiale [Groundwater flow in the material kropnozernistom]. *Izv. Nauchnoissled. Inst. Gidrotehniki (NIIG)*, Leningrad, USSR.
- Javadi, M., Sharifzadeh, M., Shahriar, K., Mitani, Y., 2014. Critical Reynolds number for nonlinear flow through rough-walled fractures: The role of shear processes. *Water Resour. Res.* 50 (2), 1789–1804.
- Jenkins, D.N., Prentice, J.K., 1982. Theory for aquifer test analysis in fractured rocks under linear (nonradial) flow conditions. *Groundwater* 20 (1), 12–21.
- Kaczmaryk, A., Delay, F., 2007. Interference pumping tests in a fractured limestone (Poitiers – France): Inversion of data by means of dual-medium approaches. *J. Hydrol.* 337 (1-2), 133–146.
- Kang, J., Jung, S., Rhee, D.Oongsub, Yeo, H., 2011. Experimental study for the determination of the material diameter of the riprap bed protection. *Engineering* 03 (10), 992–1001.
- Karpyn, Z.T., Alajmi, A., Radaelli, F., Halleck, P.M., Grader, A.S., 2009. X-ray CT and hydraulic evidence for a relationship between fracture conductivity and adjacent matrix porosity. *Eng. Geol.* 103 (3-4), 139–145.
- Kazemi, H., Seth, M.S., 1969. The interpretation of interference tests in naturally fractured reservoirs with uniform fracture distribution. *Water Resour. Res.* 9 (4), 463–472.
- Kishida, K., Sawada, A., Yasuhara, H., Hosoda, T., 2013. Estimation of fracture flow considering the inhomogeneous structure of single rock fractures. *Soils Found.* 53 (1), 105–116.
- Kohl, T., Evans, K.F., Hopkirk, R.J., Jung, R., Rybach, L., 1997. Observation and simulation of non-Darcian flow transients in fractured rock. *Water Resour. Res.* 33 (3), 407–418.
- Kuhlman, K.L., 2012. Review of inverse Laplace transform algorithms for Laplace-space numerical approaches. *Numeric. Algorith.* 63 (2), 339–355.
- Li, J., Chen, J.-J., Zhan, H., Li, M.-G., Xia, X.-H., 2020a. Aquifer recharge using a partially penetrating well with clogging-induced permeability reduction. *J. Hydrol.* 590, 125391. <https://doi.org/10.1016/j.jhydrol.2020.125391>.
- Li, Z., Wan, J., Huang, K., Chang, W., He, Y., 2017. Effects of particle diameter on flow characteristics in sand columns. *Int. J. Heat Mass Transf.* 104, 533–536.
- Li, Z., Wan, J., Zhan, H., Cheng, X.i., Chang, W., Huang, K., 2019. Particle size distribution on Forchheimer flow and transition of flow regimes in porous media. *J. Hydrol.* 574, 1–11.
- Li, Z., Wan, J., Zhan, H., He, L., Huang, K., 2020b. An energy perspective of pore scale simulation and experimental evidence of fluid flow in a rough conduit. *J. Hydrol.* 587, 125010. <https://doi.org/10.1016/j.jhydrol.2020.125010>.
- Li, J., Xia, X.-H., Zhan, H., Li, M.-G., Chen, J.-J., 2021. Non-Darcian flow for an artificial recharge well in a confined aquifer with clogging-related permeability reduction. *Adv. Water Resour.* 147, 103820. <https://doi.org/10.1016/j.advwatres.2020.103820>.
- Liu, M.-M., Chen, Y.-F., Hong, J.-M., Zhou, C.-B., 2016. A generalized non-Darcian radial flow model for constant rate test. *Water Resour. Res.* 52 (12), 9325–9343.
- Macdonald, I.F., El-Sayed, M.S., Mow, K., Dullien, F.A.L., 1979. Flow through porous media—the. *Ind. Eng. Chem. Fundam.* 18 (3), 199–208.
- Mathias, S.A., Butler, A.P., Zhan, H., 2008. Approximate solutions for Forchheimer flow to a well. *J. Hydraul. Eng.* 134 (9), 1318–1325.
- Mathias, S.A., Moutsopoulos, K.N., 2016. Approximate solutions for Forchheimer flow during water injection and water production in an unconfined aquifer. *J. Hydrol.* 538, 13–21.
- Mathias, S.A., Todman, L.C., 2010. Step-drawdown tests and the Forchheimer equation. *Water Resour. Res.* 46 (7), W07514.
- Min, K.-B., Rutqvist, J., Elsworth, D., 2009. Chemically and mechanically mediated influences on the transport and mechanical characteristics of rock fractures. *Int. J. Rock Mech. Min. Sci.* 46 (1), 80–89.
- Moench, A.F., 1984. Double-porosity models for a fissured groundwater reservoir with fracture skin. *Water Resour. Res.* 20 (7), 831–846.
- Molinero, J., Samper, J., Juanes, R., 2002. Numerical modeling of the transient hydrogeological response produced by tunnel construction in fractured bedrocks. *Eng. Geol.* 64 (4), 369–386.
- Mwetulundila, A.L., Atangana, A., 2020. Applying the Forchheimer equation to model an artificially recharged fractured aquifer. *Alexandria Eng. J.* 59 (4), 2115–2130.
- Neuzil, C.E., 1986. Groundwater flow in low-permeability environments. *Water Resour. Res.* 22 (8), 1163–1195.
- Papadopoulou, M.P., Varouchakis, E.A., Karatzas, G.P., 2009. Terrain discontinuity effects in the regional flow of a complex karstified aquifer. *Environ. Model. Assess.* 15 (5), 319–328.
- Qian, J.-Z., Wang, M.u., Zhang, Y., Yan, X.-S., Zhao, W.-D., 2015. Experimental study of the transition from non-Darcian to Darcy behavior for flow through a single fracture. *J. Hydodyn.* 27 (5), 679–688.
- Qian, J., Chen, Z., Zhan, H., Guan, H., 2011. Experimental study of the effect of roughness and Reynolds number on fluid flow in rough-walled single fractures: a check of local cubic law. *Hydropl. Process.* 25 (4), 614–622.
- Qian, J., Zhan, H., Luo, S., Zhao, W., 2007. Experimental evidence of scale-dependent hydraulic conductivity for fully developed turbulent flow in a single fracture. *J. Hydrol.* 339 (3-4), 206–215.
- Qian, J., Zhan, H., Zhao, W., Sun, F., 2005. Experimental study of turbulent unconfined groundwater flow in a single fracture. *J. Hydrol.* 311 (1-4), 134–142.
- Qian, X., Xia, C., Gui, Y., 2018. Quantitative estimates of non-Darcy groundwater flow properties and normalized hydraulic aperture through discrete open rough-walled joints. *Int. J. Geomech.* 18 (9), 04018099. [https://doi.org/10.1061/\(ASCE\)GM.1943-5622.0001228](https://doi.org/10.1061/(ASCE)GM.1943-5622.0001228).
- Quinn, P.M., Cherry, J.A., Parker, B.L., 2011. Quantification of non-Darcian flow observed during packer testing in fractured sedimentary rock. *Water Resour. Res.* 47 (9), W09533.
- Quinn, P.M., Cherry, J.A., Parker, B.L., 2020. Relationship between the critical Reynolds number and aperture for flow through single fractures: evidence from published laboratory studies. *J. Hydrol.* 581, 124384. <https://doi.org/10.1016/j.jhydrol.2019.124384>.
- Quinn, P.M., Parker, B.L., Cherry, J.A., 2013. Validation of non-Darcian flow effects in slug tests conducted in fractured rock boreholes. *J. Hydrol.* 486, 505–518.
- Radilla, G., Nowamooz, A., Fourar, M., 2013. Modeling non-Darcian single- and two-phase flow in transparent replicas of rough-walled rock fractures. *Transp. Porous Media* 98 (2), 401–426.
- Ren, F., Ma, G., Fu, G., Zhang, K.e., 2015. Investigation of the permeability anisotropy of 2D fractured rock masses. *Eng. Geol.* 196, 171–182.
- Rong, G., Hou, D.i., Yang, J., Cheng, L., Zhou, C., 2017. Experimental study of flow characteristics in non-mated rock fractures considering 3D definition of fracture surfaces. *Eng. Geol.* 220, 152–163.
- Rong, G., Yang, J., Cheng, L., Zhou, C., 2016. Laboratory investigation of nonlinear flow characteristics in rough fractures during shear process. *J. Hydrol.* 541, 1385–1394.
- Sen, Z., 1987. Non-Darcian flow in fractured rocks with a linear flow pattern. *J. Hydrol.* 92, 43–57.
- Shi, W., Yang, T., Yu, S., 2020. Experimental investigation on non-darcy flow behavior of granular limestone with different porosity. *J. Hydrol. Eng.* 25 (8), 06020004. [https://doi.org/10.1061/\(ASCE\)HE.1943-5584.0001966](https://doi.org/10.1061/(ASCE)HE.1943-5584.0001966).
- Sivanesapillai, R., Steeb, H., Hartmaier, A., 2014. Transition of effective hydraulic properties from low to high Reynolds number flow in porous media. *Geophys. Res. Lett.* 41 (14), 4920–4928.
- Skjetne, E., Auriault, J.-L., 1999. High-velocity laminar and turbulent flow in porous media. *Transp. Porous Media* 36, 131–147.
- Smaoui, H., Zouhri, L., Ouahsine, A., Carlier, E., 2012. Modelling of groundwater flow in heterogeneous porous media by finite element method. *Hydropl. Process.* 26 (4), 558–569.
- Soni, J.P., Islam, N., Basak, P., 1978. An experimental evaluation of non-Darcian flow in porous media. *J. Hydrol.* 38 (3-4), 231–241.
- Stehfest, H., 1970a. Algorithm 368: Numerical inversion of Laplace transforms [D5]. *Commun. ACM* 13 (1), 47–49.
- Stehfest, H., 1970b. Remark on algorithm 368: Numerical inversion of Laplace transforms. *Commun. ACM* 13 (10), 624. <https://doi.org/10.1145/355598.362787>.
- Talbot, A., 1979. The accurate numerical inversion of Laplace transforms. *J. Appl. Math. Mech.* 23 (1), 97–120.
- Tzelepis, V., Moutsopoulos, K.N., Papaspyros, J.N.E., Tsihrintzis, V.A., 2015. Experimental investigation of flow behavior in smooth and rough artificial fractures. *J. Hydrol.* 521, 108–118.
- Wang, H., Ju, Y., Ranjith, P. G. and Zhang, Q. (2013) Numerical Analysis of Fluid Flow in Single Rock Fracture, pp. 1769–1776.
- Wang, Q., Zhan, H., Tang, Z., 2014. Forchheimer flow to a well-considering time-dependent critical radius. *Hydrol. Earth Syst. Sci.* 18 (6), 2437–2448.
- Wang, Q., Zhan, H., Wang, Y., 2017. Single-well push-pull test in transient Forchheimer flow field. *J. Hydrol.* 549, 125–132.
- Warren, J., Root, P.J., 1963. The behavior of naturally fractured reservoirs. *Soc. Petrol. Eng. J.* 3 (3), 245–255.
- Weeks, W., 1966. Numerical inversion of Laplace transforms using Laguerre functions. *J. ACN* 13 (3), 419–429.
- Wen, Z., Huang, G., Zhan, H., 2006. Non-Darcian flow in a single confined vertical fracture toward a well. *J. Hydrol.* 330 (3-4), 698–708.

- Wen, Z., Huang, G., Zhan, H., 2008a. An analytical solution for non-Darcian flow in a confined aquifer using the power law function. *Adv. Water Resour.* 31 (1), 44–55.
- Wen, Z., Huang, G., Zhan, H., 2011. Non-Darcian flow to a well in a leaky aquifer using the Forchheimer equation. *Hydrogeol. J.* 19 (3), 563–572.
- Wen, Z., Huang, G., Zhan, H., Li, J., 2008b. Two-region non-Darcian flow toward a well in a confined aquifer. *Adv. Water Resour.* 31 (5), 818–827.
- Wen, Z., Liu, K., Chen, X., 2013. Approximate analytical solution for non-Darcian flow toward a partially penetrating well in a confined aquifer. *J. Hydrol.* 498, 124–131.
- Wen, Z., Liu, Z., Jin, M., Zhan, H., 2014. Numerical modeling of Forchheimer flow to a pumping well in a confined aquifer using the strong-form mesh-free method. *Hydrogeol. J.* 22 (5), 1207–1215.
- Wen, Z., Wang, Q., 2013. Approximate analytical and numerical solutions for radial non-Darcian flow to a well in a leaky aquifer with wellbore storage and skin effect. *Int. J. Numer. Anal. Meth. Geomech.* 37 (11), 1453–1469.
- Wen, Z., Wu, F., Feng, Q., 2016. Non-Darcian flow to a partially penetrating pumping well in a leaky aquifer considering the aquitard-aquifer interface flow. *J. Hydrol. Eng.* 21 (12), 06016011. [https://doi.org/10.1061/\(ASCE\)HE.1943-5584.0001446](https://doi.org/10.1061/(ASCE)HE.1943-5584.0001446).
- Worthington, S.R.H., Foley, A.E., Soley, R.W.N., 2019. Transient characteristics of effective porosity and specific yield in bedrock aquifers. *J. Hydrol.* 578, 124129. <https://doi.org/10.1016/j.jhydrol.2019.124129>.
- Wu, Y.-S., 2002. An approximate analytical solution for non-Darcy flow toward a well in fractured media. *Water Resour. Res.* 38 (3), 1023.
- Xia, C.-C., Qian, X., Lin, P., Xiao, W.-M., Gui, Y., 2017. Experimental investigation of nonlinear flow characteristics of real rock joints under different contact conditions. *J. Hydraul. Eng.* 143 (3), 04016090. [https://doi.org/10.1061/\(ASCE\)HY.1943-7900.0001238](https://doi.org/10.1061/(ASCE)HY.1943-7900.0001238).
- Xiao, L., Ye, M., Xu, Y., Gan, F., 2019. A simplified solution using Izbash's equation for non-Darcian flow in a constant rate pumping test. *Ground Water* 57 (6), 962–968.
- Zhan, H., Wen, Z., Gao, G., 2009. An analytical solution of two-dimensional reactive solute transport in an aquifer-aquitard system. *Water Resour. Res.* 45 (10), W10501.
- Zhang, M., Prodanović, M., Mirabolghasemi, M., Zhao, J., 2019. 3D microscale flow simulation of shear-thinning fluids in a rough fracture. *Transp. Porous Media* 128 (1), 243–269.
- Zhang, Q., 2020. Hydromechanical modeling of solid deformation and fluid flow in the transversely isotropic fissured rocks. *Comput. Geotech.* 128, 103812. <https://doi.org/10.1016/j.compgeo.2020.103812>.
- Zhang, Q., Yan, X., Shao, J., 2021. Fluid flow through anisotropic and deformable double porosity media with ultra-low matrix permeability: a continuum framework. *J. Petrol. Sci. Eng.* 200, 108349. <https://doi.org/10.1016/j.petrol.2021.108349>.
- Zhou, J.-Q., Hu, S.-H., Fang, S., Chen, Y.-F., Zhou, C.-B., 2015. Nonlinear flow behavior at low Reynolds numbers through rough-walled fractures subjected to normal compressive loading. *Int. J. Rock Mech. Min. Sci.* 80, 202–218.
- Zhu, Q., Wen, Z., 2020. Combined role of leaky and non-Darcian effects on the flow to a pumping well with a non-uniform flux well-face boundary. *J. Hydrol.* 580, 123532. <https://doi.org/10.1016/j.jhydrol.2019.02.058>.
- Zoorabadi, M., Saydam, S., Timms, W., Hebblewhite, B., 2015. Non-linear flow behaviour of rough fractures having standard JRC profiles. *Int. J. Rock Mech. Min. Sci.* 76, 192–199.